I.J. Image, Graphics and Signal Processing, 2025, 1, 45-58
Published Online on February 8, 2025 by MECS Press (http://www.mecs-press.org/)
DOI: 10.5815/ijigsp.2025.01.04

An Autoencoder-Based Deep Learning Model for Fractographic Characterization of Tungsten Heavy Alloys

Sudipta Pal
MOL IT India Pvt Ltd, Kolkata, 700091, India
E-mail: palsudipta1969@gmail.com
ORCID iD: https://orcid.org/0009-0004-8471-3346

Triparna Sarkar
Narula Institute of Technology, Kolkata, 700109, India
E-mail: triparnasarkar0683@gmail.com
ORCID iD: https://orcid.org/0009-0005-0754-4531

Sourav Saha*
Narula Institute of Technology, Kolkata, 700109, India
E-mail: souravsaha1977@gmail.com
ORCID iD: https://orcid.org/0000-0001-7242-5540
*Corresponding Author

Priya Ranjan Sinha Mahapatra
University of Kalyani, Kalyani, West Bengal, India
E-mail: priya@klyuniv.ac.in
ORCID iD: https://orcid.org/0000-0002-6943-3934

Received: 14 June, 2024; Revised: 28 August, 2024; Accepted: 10 October, 2024; Published: 08 February, 2025

Abstract: Fracture surface analysis is crucial in investigating manufacturing failures and material characterization. Traditional manual inspection methods are slow and subjective, prompting the need for efficient automated tools using advanced computer vision techniques. Recent machine learning models for classifying surface fractures show potentials but struggle due to the lack of large, labeled datasets. This study explores the potential application of autoencoders, a self-supervised neural network, to identify unintended fracture surfaces from anomalous manufacturing of tungsten-heavy alloys. The proposed autoencoder-based model achieves 97% accuracy in distinguishing undesirable fracture patterns by analyzing the reconstruction loss of the images, surpassing existing methods. This high accuracy highlights the autoencoder's ability to automatically extract and reduce dimensional features from fracture surfaces effectively. The experimental result obtained on tungsten-heavy alloys demonstrate the model's potential towards developing autoencoder-based automated tools for fractographic analyses across various materials and operational scenarios.

Index Terms: Autoencoder, Fractography, Machine Learning, Computer Vision Technique, Tungsten Heavy Alloys (WHA)

1. Introduction

Fracture surface analysis is a crucial aspect of materials characterization, providing valuable insights into the mechanisms of material failure and underlying causes. Traditional manual identification methods for fracture surfaces are time-consuming, subjective and heavily reliant on expert knowledge. However, the advent of machine learning techniques and its ability to automatically extract intricate features from raw images has paved the way for more efficient and accurate detection approaches for Undesired fracture patterns caused due to manufacturing error during production of many engineering materials which include metal alloys, concrete, polymers, ceramics etc.

Tungsten [*wolfram*] Heavy Alloys (WHA) are two-phase composites [1] with 88-98% tungsten content and alloying elements like Ni, Fe, or Cu forming the matrix. Typically, Tungsten Heavy Alloy is used in structural components in military and industrial applications where high density, high strength and ductility are required. WHAs are manufactured by various processing techniques [2] such as regular powder metallurgy, powder injection molding, microwave sintering, spark plasma sintering etc. The presence of a metal matrix along with high -tungsten content leads to excellent ductility, strength and machinability of the resulting alloy. Key mechanical properties including strength, fracture toughness and anti-corrosion characteristics, are superior in WHA with up to 97% tungsten compared to those with 99% tungsten. This improvement is attributed to a more uniform microstructure due to finer tungsten grains and a larger matrix volume fraction. As the tungsten percentage increases beyond 97%, WHA's mechanical properties decline rapidly [3]. These unique attributes make WHAs very suitable for specialized applications such as radiation shields, vibration dampers, rocket nozzles, machining tools, and electrical contacts. Hence, it is critical to distinguish between fracture surfaces of components made of standard WHAs (88-98%W) and those caused by higher tungsten levels (99%W or more) due to manufacturing errors. This differentiation is essential for preventing potential premature failures of WHA and probing the underlying causes of manufacturing issues. The conventional manual techniques for detecting the manufacturing defects involve inspection of fractured surface images. Such techniques are characterized by their labor-intensive nature, subjectivity, and significant dependence on the expertise of individuals. Imperatively, there has always been a demand for development of automated tools that can distinguish fracture patterns originating from the production failures.

In recent years, several studies have adopted computer vision-based supervised learning [4-12] approaches for the automated classification of fracture patterns using image datasets labelled by experts. However, obtaining extensive labelled data is challenging due to the labor-intensive annotation process and the wide variety of fracture patterns. Therefore, there is a need for models that can achieve desired results with limited data [5]. Some studies have utilized textural feature extraction, involving manual feature engineering, followed by various classifier algorithms such as Support Vector Machine (SVM) and Artificial Neural Network (ANN) [4], Linear Discriminant Analysis (LDA) [8], and Linear Logistic Regression [11]. This approach suffers from limited feature representation and may overlook complex patterns in the data that deep learning models can capture. In an investigation traditional deep learning and m-DAWN architectures [9] have been used on fracture surface classification and achieved an accuracy of 85-87%, In contrast, unsupervised techniques [13] eliminate the need for substantial annotation of diverse fracture patterns. However, these techniques lack a definitive similarity measure to effectively isolate undesirable fracture patterns. Therefore, the development of better and robust models that can adopt automated feature extraction and provide higher accuracy with limited dataset and without extensive labelling is anticipated in the future.

In response to these challenges, our proposed work introduces a novel approach to explore the potential application of autoencoders for fractographic analysis of metallic materials like WHA. Autoencoders are a special type of neural network model, often known as self-supervised model that can generate compressed representation of input data while retaining the essential features and attempts to reproduce the original data with minimum error from the compressed representation. The concept of using autoencoders in the context of surface defects of engineering materials has gained attention recently [18-24] due to its potential in reducing the dependency on explicit feature extraction approaches. Our proposed model is found to be capable of learning from fracture surface images through the inherent architecture of autoencoder while capturing the essential structural patterns of Desired fractured images. By computing the threshold values of reconstruction losses produced by the autoencoder module, our model effectively distinguishes between fracture images of regular WHAs (88-98%W) and those with higher tungsten content (99%W or more), as depicted in Fig.1. In comparison to existing models, our proposed model outperforms with a 97% accuracy in fracture type differentiation. This approach not only overcomes the challenges associated with traditional supervised and unsupervised learning methods but also introduces a level of accuracy that surpasses previous studies.

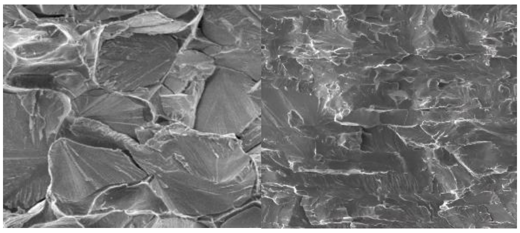

(a) (b)

Fig. 1. (a) standard desirable fracture surface image of WHA (88-98%) and (b) undesirable fracture surface image for 99%W alloy indicating anomaly

The remaining sections of the article is structured as follows. Section 2 describes the related works and the contributory scope of the proposed work on the potential application of machine learning to the fractographic study of materials. Section 3, elaborates on the proposed approaches, specifically focusing on an autoencoder- based model for detecting fracture patterns. Section 4 provides the comprehensive details of experiments, results, and analysis. The concluding remarks and avenues of further research are presented in Section 5.

2. Survey of Literature

Fractography is that branch of material science [14] wherein one studies the topographical features of fracture to characterize the various fracture modes, e.g., ductile, brittle, fatigue, corrosion or a mix of various modes depending on various intrinsic (microstructure) and extrinsic (imposed loading) conditions. Crack propagation path during fracture process leads to transgranular and intergranular fracture events. Few other attributes [15] such as grain size, orientation, defects and inclusions, phase distribution with intermetallic phases play crucial role in determining fracture behavior and related mechanism. The analysis of fractography and subsequent characterization is traditionally carried out by experts through visual inspection using a stereoscopic microscope and a Scanning Electron Microscope (SEM). Understandably, this manual approach is cumbersome, as it involves subjective judgments, making it unsuitable for quantitative analysis.

In order to present a contemporary survey of machine learning-based approaches for fractography, we focused primarily on deep learning-based solutions proposed by eminent researchers and practitioners. Mar´ıa X. Bastidas-Rodrigueza et al. [4] presented a classification model based on Artificial Neural Network (ANN) that classifies three common fracture patterns, namely, ductile, brittle and fatigue with 81-85% accuracy. Ashish Sinha and K.S Suresh proposed a novel approach [5] for dimple segmentation in quantitative fractography using deep learning techniques. Konovalenko et al. [6] successfully deployed a 4-layer CNN to investigate the rupture surface of titanium alloys like VT23 & VT23M. Detailed characterization studies using image texture analysis were conducted by Dutta S et al. [7] on various grades of stainless steel fractography and established few texture descriptors are strongly correlated with mechanical properties. In the research conducted by Dayakar L. Naik et al. [8], a Linear Discriminant Analysis (LDA) based classifier with Local Binary Pattern (LBP) as texture features was applied to categorize fracture surface images of ASTM A992 structural steel with reported accuracy of 94%. In another study by Mar´ıa X. Bastidas- Rodrigueza et al. [9] presented a deep learning approach for classifying fracture surfaces in metallic materials. They compared the performances of various Convolutional Neural Networks (CNN) and reported a F1 score of 0.864 on SEM images using a modified DAWN architecture. Stylianos Tsopanidis and team [10] formulated a pre-trained CNN with U-net architecture for semantic segmentation to examine the fracture surface of $MgAl_2O_4$ samples. Texture analysis-based approach for classifying fractures surfaces were explored by Akihiro Endo et al. [11] using Linear logistic regression and classification by voting, achieving ~90% accuracy even with small datasets. Han Yan and colleagues [12] proposed a Multi-perception Region of Interest Feature Fusion (MRIFF) method, employing deep learning techniques to recognize various metal fracture types.

As an alternative to completely supervised learning approaches as discussed before, Stylianos Tsopanidis et al. [13] proposed a hybrid framework using both unsupervised and supervised machine learning techniques for fractographic characterization of Tungsten Heavy Alloys with varying compositions. The proposed model applies clustering to the fracture patterns using k-Means algorithm and subsequently deploys k-NN classification on the clustered data points for the identification of various fracture patterns. The reported accuracy for clustering is 91%, while the accuracy for classification is 93%.

Although the use of Autoencoder-based classifiers in fractographic analysis is still very limited, they have been employed in numerous studies to recognize surface defects in various materials. These classifiers leverage automatic feature extraction to detect a wide range of defects with minimal domain expertise. Mujeeb, Abdul et al. [18] have adopted a deep autoencoder network with data augmentation to generate unique image descriptors for detecting surface level manufacturing defects through similarity matching that doesn't rely on defect samples for training. Di, He et al. [19] proposed CAE-SGAN method, combining Convolutional Autoencoder (CAE) and semi-supervised Generative Adversarial Networks (SGAN), by training on unlabeled data to enhance feature extraction and classification accuracy, and demonstrated defect detection accuracy enhancement by around 16% over traditional methods. S. Bunrit et al. [20] have demonstrated that transfer learning with pre-trained CNN models like GoogleNet and ResNet101, originally trained on ImageNet, shows high accuracy for classifying construction material images. Applying Autoencoder on top of the pre-trained transferred features, the performance can be further improved. Numerous investigations have utilized autoencoders for anomaly detection. Chow et al. [21] demonstrated a convolutional autoencoder's high accuracy and efficiency in detecting concrete defects like cracks and spalling, adapting to various conditions. Tsai et al. [22] enhanced defect detection in manufacturing and concrete structures with regularized CAEs, outperforming traditional models. Additionally, Liu et al. [23] proposed a semi-supervised method with dual prototypes autoencoder for industrial inspection, demonstrating the generalization and effectiveness of the proposed method on 4 datasets consisting of various materials, while Sun, Zhongju et al. [24] introduced random anomaly multi-scale feature focused autoencoder (RAMFAE), an unsupervised visual anomaly detection method.

2.1 Contributory Scope of the Proposed Work

Despite increasing interest in quantitative fractographic analysis of materials [10, 25, 26], the use of machine learning in this field is still emerging. While some studies have employed supervised learning-based models like CNN for fractographic analysis and semi-supervised models such as autoencoders for surface defect recognition, the application of autoencoder-based models in fractographic analysis remains very limited yet. The set of publications presented so far are indicative of the possibility of further scope of study in this specific field in view of the recent emerging deep learning-based techniques. Our proposed work is intended to leverage the power of latest machine learning concepts in the following way:

1. Application of autoencoder as one of the effective approaches in fractographic investigation.
2. Study of reconstruction loss produced by autoencoder module while applied to various fracture patterns and computation of threshold value using various thresholding techniques to distinguish fracture pattern of interest.
3. Application of the proposed model as automated fracture inspection tool for detection of probable manufacturing anomalies. The current work is an objective example of the proposed approach.

3. Proposed Work

Our research builds upon the dataset of Tsopanidis and Osovski [13]. In contrast to the data pipeline based on unsupervised clustering technique followed by k-nearest neighbor, termed as minimally supervised algorithm described in their work, our investigation presents a self-supervised algorithm, an autoencoder based computer vision model for detection of fracture patterns, processing through the dataset of SEM fracture images.

3.1 Overall Approach

The fracture pattern detection model consists of 2 modules: a) autoencoder module, to reconstruct the images from original images and b) reconstruction loss computation module, to compute the reconstruction loss for the image dataset. Loss of each fracture image is compared with threshold loss (R) obtained either by manual or automated technique and thus distinguished as Desired & Undesired fracture images. The broad view of the approach during deployment phase is depicted in Fig. 2.

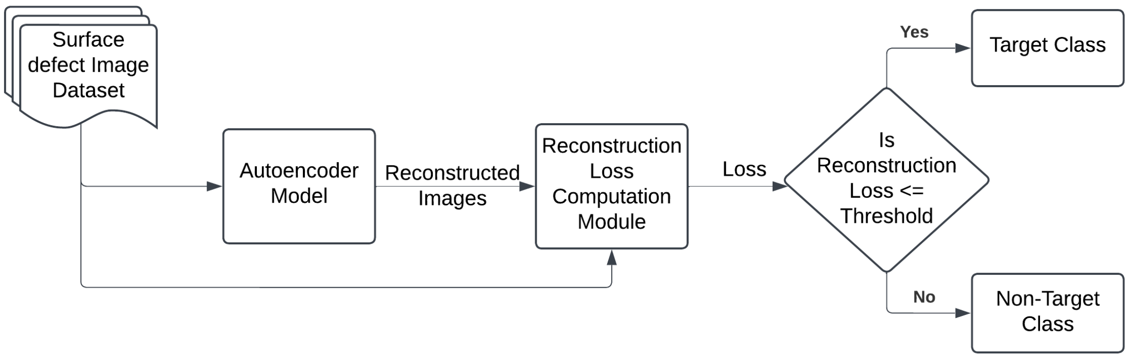

Fig. 2. Flow diagram of the proposed model during deployment phase

At the outset, fracture image dataset of WHAs (92-95-97-99%) is imported from the repository. Then the image dataset is segmented into training, validation and testing datasets. Thereby, fracture images of standard WHA (92- 95-97%), used for training the model & validating the same, termed as “Desired” class, while the same of WHA (99%), used for testing the model is termed as “Undesired” class. Training datasets are further augmented by flip technique, to increase the diversity of training data, subsequently to be fed to the proposed model. The detailed block diagram of the proposed autoencoder based fracture pattern detection model for identifying the various fracture types of WHA materials is presented in Fig 3.

The fundamental design of the proposed model centers around the use of an autoencoder approach, featuring two Convolutional (Conv) layers in both the encoder and decoder blocks, depicted in Fig. 4. In this architecture, the encoder compresses the images into a lower-dimensional latent space representation, which the decoder then utilizes to reconstruct the original images. During training, only Desired class images are used to create a lower- dimensional latent space representation, minimizing reconstruction loss discrepancies. The rationale behind this approach is that during testing, the decoder's reconstruction of Desired class images from the latent space representation will exhibit lower reconstruction loss compared to Undesired class images. Consequently, following training, testing datasets comprising of both Desired and Undesired images are reconstructed to compute reconstruction losses.

Subsequently, a histogram representing the frequency distribution of the reconstruction loss for each test image is presented in Fig. 6. An optimal threshold value, denoted as R, is determined through analysis of the frequency distribution curve, using both manual and automated threshold determination techniques. The determined value of "R" is subsequently utilized to categorize test images. If the reconstruction loss of an image falls within the threshold, it is predicted to belong to the Desired class; otherwise, it is categorized as belonging to the Undesired class**.** This process ensures effective detection of Undesired class of images between different fracture types in WHA materials.

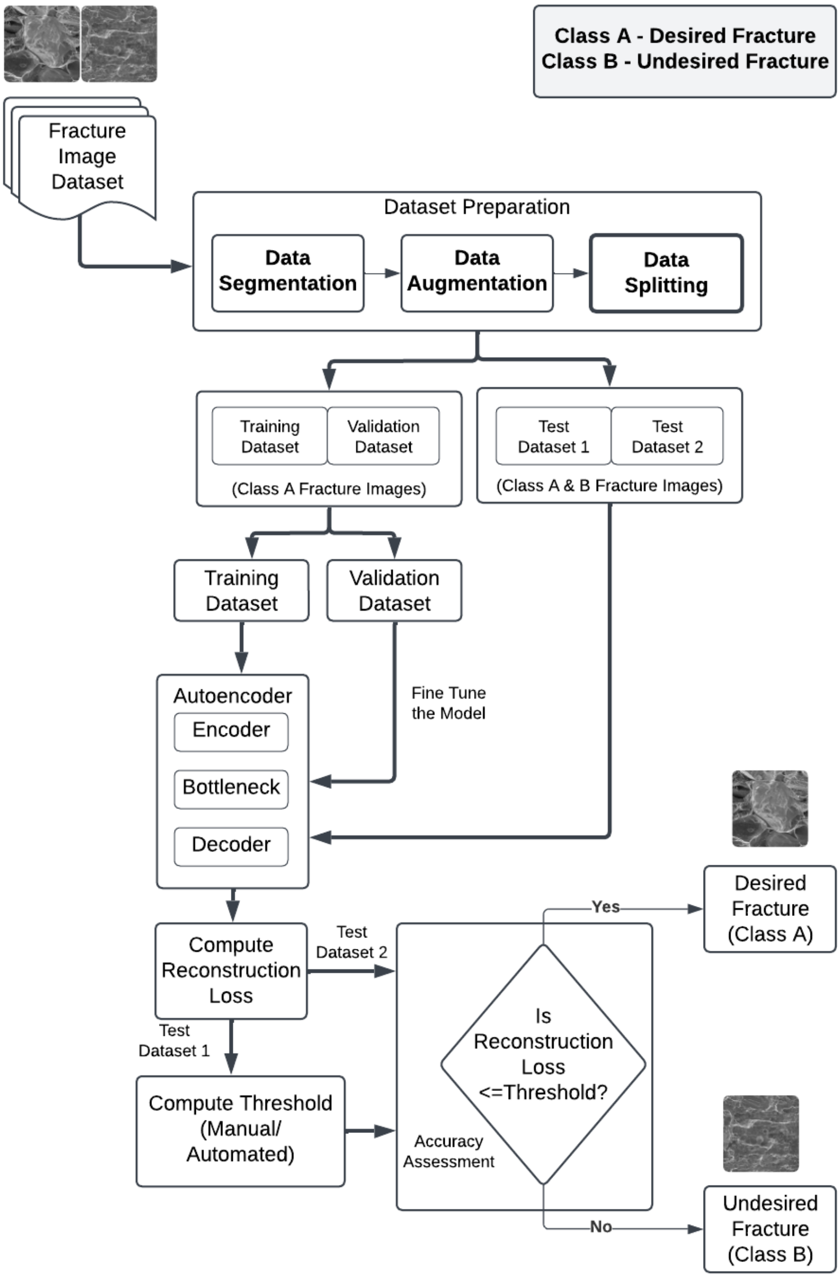

Fig. 3. Block diagram of proposed approach

3.2 Autoencoder based Fracture Pattern Detection Model

Autoencoders are a special type of feed forward neural networks where output is same as input. They compress the input into a lower dimensional code and then reconstructs the output from this representation. An autoencoder consists of 3 components – encoder, code and decoder- while encoder compresses the image and produces the code, decoder reconstructs the image using the code. Hence reconstruction loss is an indicator of training efficacy and thus a self-supervised trained autoencoder can be considered as binary classifier for Desired class.

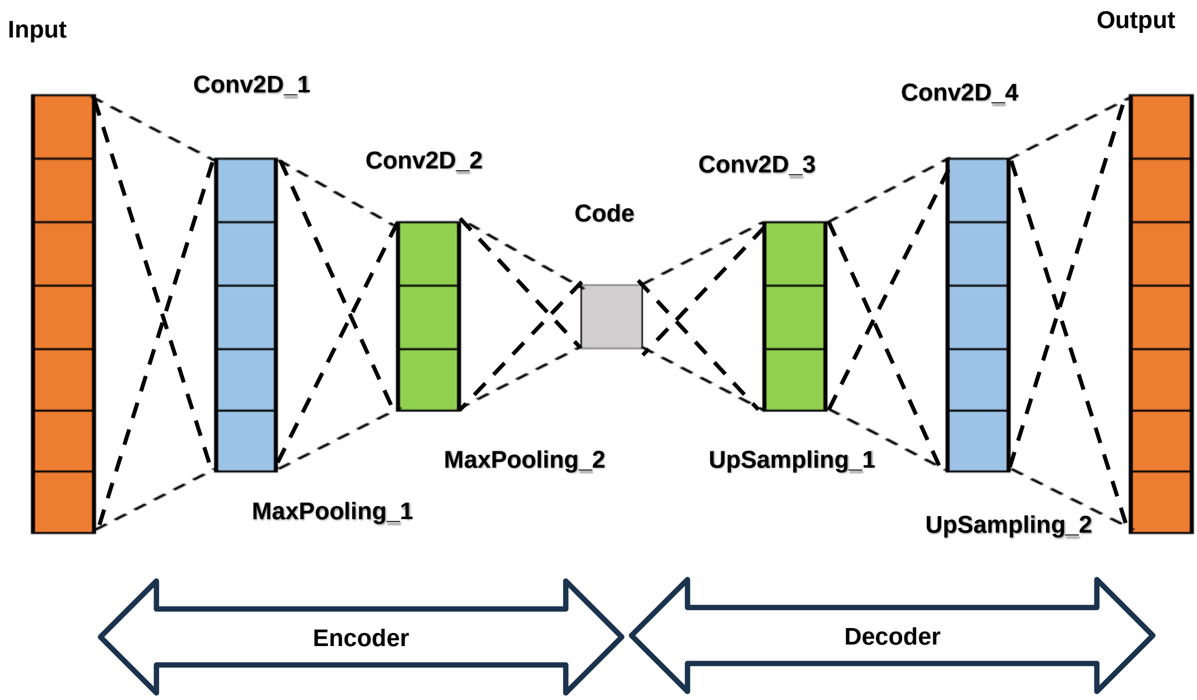

Fig. 4. Autoencoder architecture

Network architecture:

An autoencoder network architecture typically consists of a sequence of encoder and decoder parts. Fig. 4 illustrates an autoencoder architecture, with its structural specifications provided in Table 1. The encoder part of the autoencoder consists of two convolutional layers with 16 and 8 filters respectively. Each convolutional layer is followed by a MaxPooling layer with a 2X2 pool size which reduces the spatial dimensions of the input feature maps. The decoder part mirrors the encoder architecture. It starts with a Convolutional layer with 8 filters, followed by an UpSampling layer with a 2x2 size to increase the spatial dimensions. Next, there is another Convolutional layer with 16 filters and an UpSampling layer. Finally, the decoder ends with a Convolutional layer with 1 filter and a sigmoid activation function to reconstruct the original input image.

Table 1. Overview of autoencoder network architecture parameters shown in Fig. 4

Layer Name	Structural Overview of the Layer
Conv2D	Filters: 16/ 8/ 1; Kernel size: 3x3; Strides: 1x1; Padding: Same; Activation: RELU/ Sigmoid
MaxPooling2D	Pool size: 2x2; Strides: 2x2; Padding: Same
UpSampling2D	Size: 2x2

The autoencoder network architecture parameters shown in Fig. 4 are outlined in Table 1 wherein the size of the kernel, used in Conv2D layers is 3x3, meaning the filter analyzes small 3x3 pixel regions of the input at a time. Strides are set to 1x1, meaning the filter moves one pixel at a time. "Same" padding ensures the output size is the same as the input by adding padding around the borders. Rectified Linear Unit (RELU) activation function is used for most of the layers, introducing non-linearity, in contrast to Sigmoid activation function which is ideal for tasks like image reconstruction.

The proposed autoencoder model learns to encode the input image into a lower-dimensional representation and then decode it back to reconstruct the original image. Therefore, if an image of 448 x 448 pixels is fed into the encoder as input, an image of 448 x 448 pixels is generated as the final output, with a progression of the output shape of the image at each layer of autoencoder as shown in Fig. 5.

While the ultimate Conv layer of the autoencoder deploys a Sigmoid activation function, as it suits binary classification, the remaining Conv layers of the encoder and decoder include a Rectified Linear Unit (ReLU) activation function. This choice is motivated by its acknowledged advantages, including faster convergence during training and prevention of the vanishing gradient problem. Identical padding is used to ensure the spatial dimensions of the input and output feature maps remain the same.

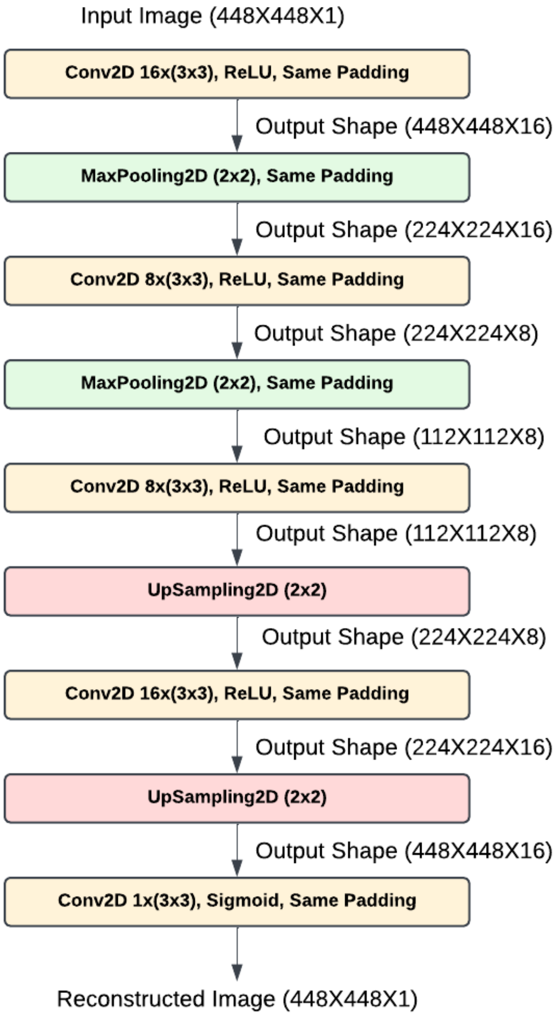

Fig. 5. Detailed Network architecture and output shape of each image at each layer

Reconstruction loss:

Initially, the autoencoder was trained on the training dataset and its performance was evaluated on the validation dataset by calculating the reconstruction loss. Training dataset and validation dataset, as described in the diagram Fig.3, both belong to Desired class image dataset.

The reconstruction loss, representing the difference between the original test images and their reconstructed counterparts, used as a performance metric to evaluate how well the autoencoder can reconstruct the test data, was computed, indicated as Mean Reconstruction Loss (MRL) as below:

$$\mathrm{MRL} = \frac{1}{n}\sum_{i=1}^{n}(XtestImg_i - ReconImg_i)^2 \quad (1)$$

Where:

- n is the number of samples in the test set
- $XtestImg_i$ represents the i-th sample in the test set
- $ReconImg_i$ represents the reconstructed image of the i-th sample from the autoencoder model

Threshold selection:

After completing the model training phase and processing the test dataset through the trained model, histogram of the test data, representing the frequency of each reconstruction loss is plotted. The resulting frequency distribution curve of reconstruction loss values is examined to determine the optimal threshold value, denoted as "R," shown in Fig.6. Two threshold determination methods are employed, as follows:

(a) One method adopts **manual determination** through visual observation of the histogram of reconstruction loss, where threshold is calculated optimally (valley between the peaks) so that False Positive (FP) and False Positive (FN) are minimized.

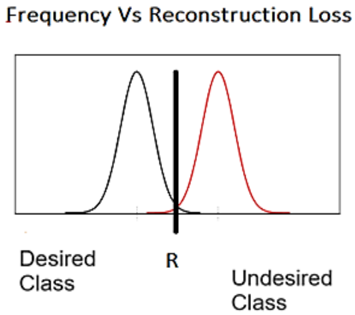

Fig. 6. Selection of reconstruction loss threshold (R) for Desired & Undesired class of images

The determined value of "R" is then used to classify test images: if an image's reconstruction loss is within the threshold "R," it is predicted to belong to the Desired class; otherwise, it is categorized as Undesired class.

(b) Another method employs an **automated thresholding** technique derived from Kapur's [16-17] and Otsu [27] histogram threshold. Kapur's thresholding effectively adapts to varying data distributions, making it ideal for datasets with overlapping or ambiguous class boundaries. This is an entropy-based approach where entropy of Desired & Undesired classes is computed as:

$$H_{\omega_D}(t) = -\sum_{i=0}^{t} \frac{p_i}{p_{\omega_D}} \log_2 \left(\frac{p_i}{p_{\omega_D}}\right) \text{ and } H_{\omega_U}(t) = -\sum_{i=t+1}^{L-1} \frac{p_i}{p_{\omega_U}} \log_2 \left(\frac{p_i}{p_{\omega_U}}\right) \quad (2)$$

Where:

- $H_{\omega_D}(t)$ is the entropy of distribution of Desired classes and $H_{\omega_U}(t)$is the entropy of distribution of Undesired classes
- p(i) is the probability of reconstruction loss of i-th bin
- p_{ω_D}& p_{ω_U} are the total probabilities for each range
- t is the threshold candidate during the process of finding the optimal threshold
- L is the highest reconstruction loss
- τ is the final optimal threshold that maximizes the sum of entropies of two probability distributions (Desired and Undesired classes).

This method calculates the final optimal threshold (τ) based on the probability distributions and entropy values derived from the reconstruction losses. This τ is then used to classify images into desired and undesired classes.

While manual thresholding offers control and more intuitive, it is time consuming for large datasets and complex histogram. Therefore, our proposed model includes the automated threshold using Kapur’s threshold approach, which reduces the need for manual intervention and subjectivity. This method is preferred over other automated thresholding methods due to its robustness against noise.

4. Experiments, Results & Performance Analysis

4.1 Dataset

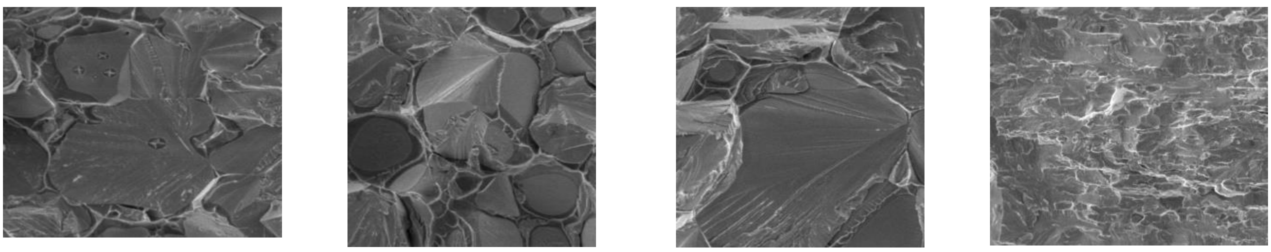
(a) (b) (c) (d)

Fig. 7. (a) Three random SEM image samples of (a) 92%W, (b) 95%W, (c) 97%W, each belonging to specific mass% W, (d) One random SEM image sample of 99%W showing undesirable fracture

Different samples belonging to different compositions of Tungsten Heavy Alloys are produced and undergo a tensile testing process at a strain rate of 1000 S^{-1}. Subsequently, the fracture surfaces originating from the tensile testing process are scanned using SEM and an image dataset with each image dimension of 448 x 448 pixels are prepared by cropping the original SEM images.

In our experimentation, a similar dataset is imported from the publicly available data repository mentioned in the acknowledgement section. The dataset of 648 SEM images containing the fracture patterns is divided into four distinct classes corresponding to four different compositional percentages of tungsten e.g., 92%, 95%, 97%, and 99%. There are 162 images in each class representing a specific compositional percentage of tungsten. Fig. 7 presents fracture images of four classes corresponding to four different compositional percentages of tungsten e.g., 92%, 95%, 97%, and 99%.

SEM images belonging to the mass percentages of tungsten at 92%, 95%, and 97% corroborate the typical fracture characteristics of standard WHAs (trans-granular cleavage and intergranular brittle fracture with matrix rupture) and all exhibit similar surface morphology [13]. In contrast, SEM images corresponding to the 99% mass percentages of tungsten predominantly exhibit distinct brittle features that differ from other categories (Fig. 7).

In view of the above-mentioned factual observation, a total of 486 images (belonging to the typical 92–95– 97% WHA category) are clubbed together and designated as Desired class "T" while the remaining 162 images (belonging to the 99% W category) are designated as Undesired class "F". The images of class T are split into a typical 80-20 ratio for training and validation of the autoencoder model. Hence, a total of 389 images are used for training the model, while the remaining 97 images are used for validating the training efficacy.

4.2 Data Augmentation and Preprocessing

In order to increase the size of our training dataset and improve the generalization capability of model, each image of the dataset belonging to the 92-95-97% W category (486 images) is flipped vertically (upside-down; mirrors images along the horizontal axis with a 100% chance) to generate a total of 972 images. Simpler technique like flipping was chosen to introduce orientation variation while preserving image features. Therefore, eventually, 778 images are used for training the model and 194 images are used for validation purposes.

The images undergo preprocessing, including resizing to 224x224 pixels, converting to grayscale, and applying a 5x5 Gaussian blur to reduce noise. Resizing ensures compatibility with the autoencoder model, and blurring aids in noise reduction.

4.3 Key Parameters used in Training the Autoencoder

An optimizer is a critical component in training the machine learning models as it plays a key role in determining how the model updates its weights to achieve better results. Additionally, loss functions also play a crucial role in guiding the training process by allowing the model to adjust its parameters during the training process to minimize the reconstruction loss of the autoencoder model.

In the Fig.8 (a), it is evident that Adaptive Moment Estimate (ADAM) optimizer leads to optimally lesser loss, thus in turn leading to faster convergence over Stochastic Gradient Descent (SGD) optimizer. Similarly, it is found in the Fig.8 (b), though BCE Loss function is often used for binary classification tasks, MSE Loss function is preferred in our proposed work as it results in much lesser loss.

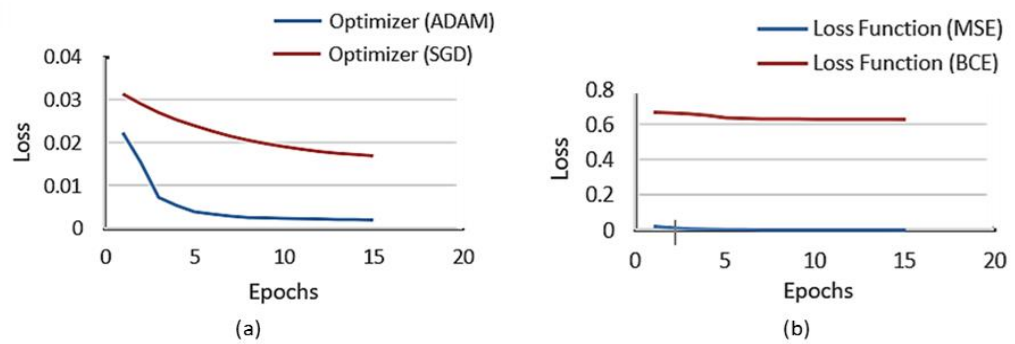

Fig. 8. Loss over training using Autoencoder model (a) with ADAM & SGD optimizer, (b) with Mean Squared Error (MSE) & Binary Cross-Entropy (BCE) loss function

Fig. 9 illustrates the loss and accuracy metrics throughout the training phase of the autoencoder. The graph reveals a consistent decline in loss as the number of epochs increases, ensuring a progressive learning capability of the model. It is further observed that loss during training reaches an optimally low at around epoch 15. This suggests that the model has already learned the underlying patterns in the data, and its effectiveness would not increase significantly with a greater number of epochs.

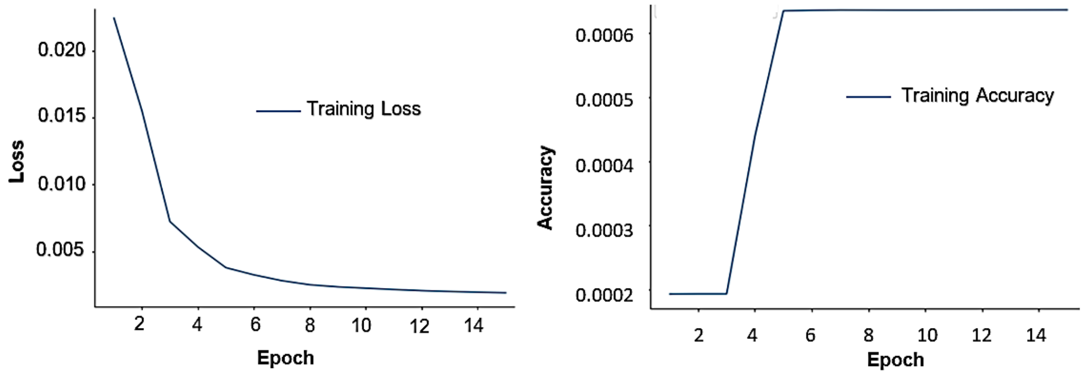

Fig. 9. Loss & accuracy over training using autoencoder

4.4 Differentiation of Fracture Pattern based on Reconstruction Loss

Frequency distribution of reconstruction loss is plotted for image dataset belonging to Desired classes and Undesired classes as shown in Fig. 10. Reconstruction loss of Desired dataset of images is found to be 0.0016 and the same for Undesired dataset of images is found to be 0.0029. Therefore, by observing the reconstruction loss of individual Desired and Undesired classes as well as the frequency distribution, the threshold R may be determined optimally so that the number of FPs and FNs are minimized in case of manual thresholding. Similarly, in Automated thresholding. optimal threshold is determined by maximizing entropy leading to more effective discrimination between different classes.

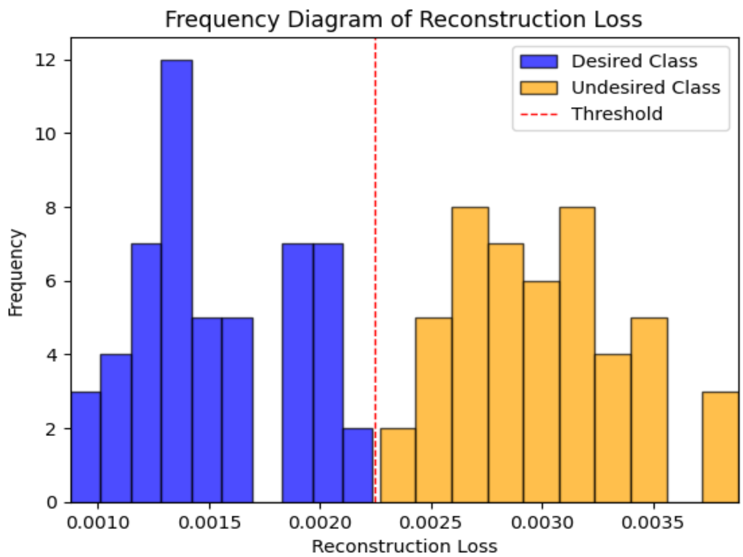

Fig. 10. Frequency distribution of reconstruction loss & categorization using threshold

Once the threshold is computed either manually or automatically, images with reconstruction loss below the threshold value are classified as Desired class, while images with reconstruction loss above the threshold value are classified as Undesired class.

4.5 Performance Analysis

The model is evaluated using a holdout validation approach where 100 test images, equally divided between the Desired class T and the Undesired class F, which are not part of the training data. The performance of the model is analyzed with Confusion Matrix as well as using various assessment metrics including precision, recall, F1 score, accuracy and Receiver Operating Characteristic (ROC). ROC is often used as single-value metric to summarize the overall performance of the model and ranges from 0 to 1. The higher the ROC value, the better is the model's ability to discriminate between positive and negative instances suggesting better performance.

Using manual threshold:

The confusion matrix, reveals that the model achieves an accuracy of 97%, with 48 correctly detected instances of class T and 49 correctly detected instances of class F (Table 2).

Table 2. Confusion matrix of fracture image detection using proposed model

Actual vs Predicted	Actual Desired Class T	Actual Undesired class F
Predicted Desired class T	48	2
Predicted Undesired class F	1	49

The precision, recall, and F1 score for class T were found to be 95%, 100%, and 97% respectively (Table 3). Certain erroneous predictions of False positive (FP) and False Negative (FN) images along with ROC curve are presented in Fig. 11.

Table 3. Performance on fracture image detection using proposed model (Desired Class)

Precision	Recall	F1 Score	Accuracy
95%	100%	97%	97%

Images with indices 57 and 96 (belonging to Undesired class) have been falsely identified as Desired class (FP) by the model with repeated tests on the dataset, while image with index 97 has been falsely identified as Desired class (FP) once. Closure scrutiny on the images reveals that the presence of multiple transgranular cleavage (marked through arrow) may lead the model to do so. Limited presence of similar feature in image with index 97 leads to its occasional failure as FP. This confirms the effectiveness of the proposed fracture pattern detection model satisfactorily.

False Positive [Indices: 57, 96, 97-Test dataset]
False Negative [Indices: -Test dataset]

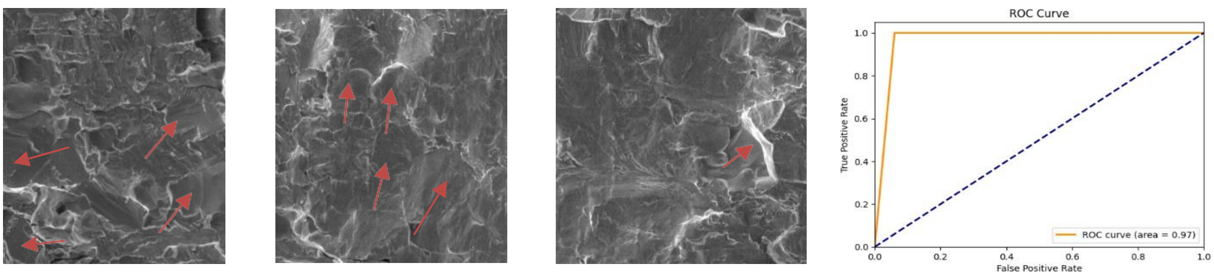

(a) (b)

Fig. 11. (a) FP & FN instances by proposed model, (b) ROC curve

Using automated threshold:

In Table 4, the results of applying both manual and automated thresholding techniques (Otsu and Kapur) are compared, including various performance parameters.

Table 4. Threshold and other performance parameters using manual and automated threshold

Technique	Threshold	Precision	Recall	F1 Score	Accuracy
Manual Thresholding	0.0022	0.9467	1.0000	0.9733	0.9733
Automated (Otsu's) Thresholding	0.0023	0.9453	0.9577	0.9514	0.9533
Automated (Kapur's) Thresholding	0.0021	0.9600	0.9667	0.9633	0.9633

Manual thresholding technique achieved perfect recall (1.0000), meaning it identified all true positive. The F1 score (0.9733) and accuracy (0.9733) were slightly higher than the automated method, suggesting a slight overall performance edge of manual thresholding over automated one. On other hand, automated thresholding technique had slight edge in precision (0.9600), indicating few lesser false positives besides saving manual effort. The small differences in performances suggest that either method could be viable depending on the specific needs.

4.6 Performance comparison

Table 5 presents a performance comparison between proposed autoencoder based model and other existing models. The proposed autoencoder based model showcases superior performance with an accuracy of 97% highlighting its effectiveness for fracture image detection in metallic materials.

Table 5. Performance comparison of the proposed model with other models

Model	Key Module	Performance Measure
Stylianos Tsopanidis et al. (2021) [13]	VGG-16, PCA, t-SNE, k-Means and KNN	Accuracy: 93%
Akihiro Endo et al. (2022) [11]	Textural feature extraction, Linear logistic regression, classification by voting (a) Low magnification situation (b) High magnification situation	(a) Accuracy: 90% Precision, Recall, F1 Score > 0.8 (b) Accuracy: 87% Precision, Recall, F1 Score > 0.9
M.X. Bastidas-Rodriguez (2020) [9]	(a) ResNet– 18 (b) DenseNet – 21 (c) M-DAWN	(a) Accuracy: 85.48%, F1 score: 0.848 (b) Accuracy: 81.45%, F1 score: 0.802 (c) Accuracy: 87.10%, F1 score: 0.864
Dayakar L. Naik et al. (2019) [8]	Linear Binary pattern (LBP), texture quantification algo with LDA classifier	Accuracy: 94%
M.X. Bastidas-Rodriguez (2016) [4]	(a) Textural feature extraction, SVM (b) Textural feature extraction, ANN	(a) Accuracy: 75-79%, Sensitivity: 68-93%, Specificity: 72-81% (b) Accuracy: 81-85%, Sensitivity: 64-92%, Specificity: 82-91%
Proposed Model	Autoencoder, thresholding on reconstruction loss (a) Manual thresholding (b) Automated thresholding	(a) Accuracy: 97%, Precision: 0.9467, Recall: 1.0, F1 score: 0.9733 (b) Accuracy: 96%, Precision: 0.9600, Recall: 0.9667, F1 score: 0.9633

The combination of unsupervised learning which automatically extracts relevant features from fracture images, more effective feature extraction through dimensionality reduction, and thresholding on reconstruction loss which provides a mechanism to fine tune the boundaries appear to contribute to the superior performance observed in the proposed model.

5. Conclusion

In this study, we implemented an autoencoder-based fracture pattern detection model for Tungsten Heavy Alloys with different compositions. The model achieved a high accuracy of 97%, with precision, recall, and F1 score values over 90% for both Desired and Undesired fracture classes using both manual and Kapur's automated thresholding methods. The minor differences in performance involving two thresholding methods suggest either of the thresholding method could be viable depending on specific needs.

These autoencoder-based classifiers automatically extract features to detect various fracture types with minimal domain expertise, making them highly effective tools for fractographic analysis. They identify manufacturing errors by detecting undesired fracture classes within desired ones, aiding in understanding the causes of failure in WHA-based structural components.

This model can be extended in future studies to detect various types of fractures in different structural materials, not limited to metals. It can identify fractures resulting from manufacturing errors and different fracture patterns and failure modes, such as ductile versus brittle fractures, progressive failures like fatigue, corrosion fatigue, creep, and mixed fracture modes. Additionally, it can segment fracture surface types where one fracture type overlaps and transitions to another. This characterization framework aims to detect, identify, recognize, and segment various fracture types, enhancing the understanding of underlying failure mechanisms of materials, thereby contributing to significant advancements in structural engineering.

Acknowledgement

Funding: The authors declare that no funds, grants, or other support were received during the preparation of this manuscript.

Conflict of Interest: The authors declare no conflict of interest.

Availability of data and material: The image dataset used for this study are imported from published dataset in Materials Data Facility (MDF) with DOI: https://doi.org/10.18126/aph0-olbz [13].

Code availability: Not applicable

Author contributions: First author & corresponding author claim the major contribution of the paper including formulation, analysis and editing. The other co-authors provided assistance towards preparing and verifying the results and editing the manuscript.

Compliance with ethical standards: This article is a completely original work of its authors; it has not been published before and will not be sent to other publications until the journal’s editorial board decides not to accept it for publication.

References

[1] N. Senthilnathan, A. Raja Annamalaia, G. Venkatachalama, "Microstructure and mechanical properties of spark plasma sintered Tungsten Heavy Alloys", Materials Science & Engineering A, vol. 710, pp. 66-73, 2018.

[2] Y. Sahin, "Recent Progress in Processing of Tungsten Heavy Alloys", Journal of Powder Technology, 2014, “doi: 10.1155/2014/764306”.
[3] Zhi-Bo Li, He Zhang, Guo-Hua Zhang, And Kuo-Chih Chou, "Fabrication and Characterization of Tungsten Heavy Alloys with High W Content by Powder Metallurgy", Materials Science & Engineering A, vol. 53, pp. 1085- 1098, 2022, “doi: 10.1007/s11661-021-06579-w”.
[4] M.X. Bastidas-Rodriguez, F.A. Prieto-Ortiz and Edgar Espejo, “Fractographic classification in metallic materials by using computer vision”, Engineering Failure Analysis, vol. 59, pp. 237-252, 2016, “doi: 10.1016/j.engfailanal.2015.10.008”.
[5] Ashish Sinha & K.S Suresh, "Deep Learning based Dimple Segmentation for Quantitative Fractography",
[6] Electrical Engineering and Systems Science, vol. 3, 2018, “doi: 10.48550/arXiv.2007.02267”.
[7] Konovalenko, I., Maruschak, P., Prentkovskis, O. and Junevi˘cius, R., "Investigation of the Rupture Surface of the Titanium Alloy Using Convolutional Neural Networks", Materials, vol. 11(2), p 2467, 2018, “doi: 10.3390/ma11122467”.
[8] Dutta, Samik, Arpan Das, Kaustav Barat, and Himadri Roy. "Automatic characterization of fracture surfaces of AISI 304LN stainless steel using image texture analysis", Measurement, vol. 45, no. 5, pp.1140-1150, 2012, “doi: 10.1016/j.measurement.2012.01.026”.
[9] Dayakar L. Naik and Ravi Kiran, “Identification and Characterization of Fracture in Metals using Machine Learning based Texture Recognition Algorithms”, Engineering Fracture Mechanics, vol. 219, p 106618, 2019, “doi: 10.1016/j.engfracmech.2019.106618”.
[10] Mar´ıa X. Bastidas-Rodrigueza, Luisa F. Polania, Adrien Gruson, and Flavio Prieto-Ortiz, "Deep Learning for Fractographic Classification in Metallic Materials", Engineering Failure Analysis, vol. 113, pp. 104532, 2020, “doi: 10.1016/j.engfailanal.2020.104532”.
[11] Stylianos Tsopanidis, Ral Herrero Moreno & Shmuel Osovski, "Toward quantitative fractography using convolutional neural networks", Engineering Fracture Mechanics, vol. 231, p 106992, 2020, “doi: 10.1016/j.engfracmech.2020.106992”.
[12] Akihiro Endo, Yoshiyuki Furuya, Kenji Nagata, Hideki Yoshikawa and Hayaru Shouno, "Fracture mode classification by texture analysis of fracture surface scanning electron microscope images", Science and Technology of Advanced Materials: Methods, vol. 2(1), pp. 129-138, 2022, “doi: 10.1080/27660400.2022.2065185”.
[13] Han Yan, Chongquan Zhong, Wei Lu & Yuhu Wu, "Metal fracture recognition: a method for multi- perception region of interest feature fusion", Applied Intelligence, pp. 1-25, 2023, “doi: 10.1007/s10489-023-04795-y”.
[14] Stylianos Tsopanidis and Shmuel Osovski, "Unsupervised Machine Learning in Fractography: Evaluation and Interpretation", Materials Characterization, vol. 182, p 111551, 2021, “doi: 10.18126/aph0-olbz”.
[15] Hull, Derek. Fractography: observing, measuring and interpreting fracture surface topography. Cambridge University Press, 1999.
[16] ASM Handbook, Fractography, vol. 12, “doi: 10.31399/asm.hb.v12.9781627081818”.
[17] J.N. Kapur, P.K. Sahoo and A.K.C. Wong, “A new method for gray-level picture thresholding using the entropy of the histogram”, Computer Vision, Graphics, And Image Processing, vol. 29, pp. 273-285, 1985, “doi: 10.1016/0734-189X(85)90125-2”.
[18] Roy, Moumita, Sukanta Majumder, Anindya Halder, and Utpal Biswas. "ECG-NET: A deep LSTM autoencoder for detecting anomalous ECG", Engineering Applications of Artificial Intelligence, vol. 124, p 106484, 2023, “doi: 10.1016/j.engappai.2023.106484”.
[19] Mujeeb, Abdul, Wenting Dai, Marius Erdt, and Alexei Sourin. "Unsupervised surface defect detection using deep autoencoders and data augmentation." In 2018 International conference on cyberworlds (CW), pp. 391-398. IEEE, 2018, “doi: 10.1109/Cw.2018.00076”.
[20] Di, He, Xu Ke, Zhou Peng, and Zhou Dongdong. "Surface defect classification of steels with a new semi- supervised learning method." Optics and Lasers in Engineering, vol. 117, pp. 40-48, 2019, “doi: 10.1016/j.optlaseng.2019.01.011”.
[21] S. Bunrit, N. Kerdprasop, and K. Kerdprasop. ”Improving the Representation of CNN Based Features by Autoencoder for a Task of Construction Material Image Classification”, Journal of Advances in Information Technology, vol. 11(4), 2020, “doi: 10.12720/jait.11.4.192-199”.
[22] Chow, Jun Kang, Zhaoyu Su, Jimmy Wu, Pin Siang Tan, Xin Mao, and Yu-Hsing Wang. "Anomaly detection of defects on concrete structures with the convolutional autoencoder", Advanced Engineering Informatics, vol. 45, p 101105, 2020, “doi: 10.1016/j.aei.2020.101105”
[23] Tsai, Du-Ming, and Po-Hao Jen. "Autoencoder-based anomaly detection for surface defect inspection", Advanced Engineering Informatics, vol. 48, p 101272, 2021, “doi: 10.1016/j.aei.2021.101272”.
[24] Liu, Jie, Kechen Song, Mingzheng Feng, Yunhui Yan, Zhibiao Tu, and Liu Zhu. "Semi-supervised anomaly detection with dual prototypes autoencoder for industrial surface inspection", Optics and Lasers in Engineering, vol. 136, p 106324, 2021, “doi: 10.1016/j.optlaseng.2020.106324”.
[25] Sun, Zhongju, Jian Wang, and Yakun Li. "RAMFAE: a novel unsupervised visual anomaly detection method based on autoencoder", International Journal of Machine Learning and Cybernetics, vol. 15, pp. 355–369, 2024, “doi: 10.1007/s13042-023-01913-7”.
[26] Jafari, Abouzar, Lingyue Ma, Amir Ali Shahmansouri, and Roberto Dugnani. "Quantitative fractography for brittle fracture via multilayer perceptron neural network", Engineering Fracture Mechanics. vol. 291, p 109545, 2023, “doi: 10.1016/j.engfracmech.2023.109545”.
[27] Li, Diyuan, Zida Liu, Quanqi Zhu, Chenxi Zhang, Peng Xiao, and Jinyin Ma. "Quantitative Identification of Mesoscopic Failure Mechanism in Granite by Deep Learning Method Based on SEM Images", Rock Mechanics and Rock Engineering, vol. 56, no. 7, pp. 1-22, 2023, “doi: 10.1007/s00603-023-03307-1”.
[28] P. Roy, S. Dutta, N. Dey, G. Dey, S. Chakraborty and R. Ray, "Adaptive thresholding: A comparative study," 2014 International Conference on Control, Instrumentation, Communication and Computational Technologies (ICCICCT), Kanyakumari, India, 2014, pp. 1182-1186.

Authors' Profiles

Sudipta Pal was born in Asansol, West Bengal, India in 1969. He earned an M. Tech in Metallurgical Engineering from IIT- Kharagpur, India in 1996, followed by a Post Graduate Diploma in Software Technology from NCST, Mumbai, India in 1999.

He has over three decades of industrial experience. He began his career as a Scientific Officer at BARC, Mumbai and has since worked in numerous reputed IT organizations in various roles and cross-cultural environments worldwide, leading several transformation projects. Currently, he is involved in Data Analytics and Machine Learning projects at MOL IT, Kolkata, India

Mr. Pal holds multiple professional certifications, including PMP from PMI, USA, CSQA from QAI, USA, and CMMi auditor from SEI, Carnegie Mellon University, USA.

Triparna Sarkar was born in Kolkata, India, in 2000. She completed her bachelor's degree in Computer Science and Engineering from Narula Institute of Technology, West Bengal, India. During her undergraduate studies, she was fascinated with the latest research activities in the fields of Artificial Intelligence, Machine Learning, and Image processing.

Sourav Saha was born in Kolkata, India, in 1977. He was awarded Ph.D degree in 2019 from University of Kalyani (West Bengal, India) in Computer Science & Engineering. He obtained his Master of Engineering (M.E.) degree in Computer Science and Engineering from Indian Institute of Engineering Science and Technology (– Formerly known as Bengal Engineering and Science University, West Bengal, India) in 2002 and did his graduation (B. Tech) in Computer Science & Engineering from Kalyani Govt. Engineering College (Kalyani University, West Bengal, India) in 2000.

He is currently working as a Professor in the Department of Computer Science & Engineering at Narula Institute of Technology. He started his career working in the R & D sector of various software companies for around ten years before joining academia. Since 2011, he has been associated with multiple engineering institutes and published many research articles in international journals and conferences. Currently, his area of research interest includes Computer Vision, Soft Computing, and Machine Learning.

Priya Ranjan Sinha Mahapatra has done his PhD work at Advanced Computing and Microelectronics Unit of Indian Statistical Institute, Kolkata, and received his PhD degree from University of Kalyani. He is now a Professor at the Department of Computer Science and Engineering, University of Kalyani, India.

He has numerous international and national publications in reputed journals and conferences. He has also worked as reviewer of various international journals and conferences. His research interests include Computational geometry, Graph labelling, Facility location and Image processing for facility placement.

How to cite this paper: Sudipta Pal, Triparna Sarkar, Sourav Saha, Priya Ranjan Sinha Mahapatra, "An Autoencoder-Based Deep Learning Model for Fractographic Characterization of Tungsten Heavy Alloys", International Journal of Image, Graphics and Signal Processing(IJIGSP), Vol.17, No.1, pp. 45-58, 2025. DOI:10.5815/ijigsp.2025.01.04